Transmission electron microscopy and Monte Carlo simulations of ordering in Au-Cu clusters produced in a laser vaporization source

B. Pauwels* and G. Van Tendeloo
Elektronenmicroscopie voor Materiaalonderzoek, Universiteit Antwerpen (RUCA), Groenenborgerlaan 171, B-2020 Antwerpen, Belgium

E. Zhurkin† and M. Hou
Physique des Solides Irradiés CP234, Université Libre de Bruxelles, Boulevard du Triomphe, B-1050 Bruxelles, Belgium

G. Verschoren, L. Theil Kuhn,‡ W. Bouwen,§ and P. Lievens
Laboratorium voor Vaste-Stoffysica en Magnetisme, Katholieke Universiteit Leuven, Celestijnenlaan 200 D, B-3001 Leuven, Belgium
(Received 13 September 2000; revised manuscript received 27 November 2000; published 27 March 2001)

Au-Cu bimetallic alloy clusters are produced in a laser vaporization source starting from Au-Cu alloy targets with different stoichiometric compositions. The clusters are deposited on two different substrates—amorphous carbon and crystalline MgO—and are characterized by electron diffraction and high-resolution electron microscopy. The experiments show that the overall chemical composition in the clusters is the same as the chemical composition of the target material; but the crystal structure of the Au-Cu alloy clusters differs from their known bulk crystal structure. Electron microscopy experiments provide evidence that no chemical ordering exists between Au and Cu atoms and that the clusters are solid solutions. Monte Carlo simulations using the second moment tight-binding approximation, however, predict Cu_3Au clusters ordered in the core but with a disordered mantle. The possible origins of the differences between experiment and Monte Carlo simulations are discussed.

DOI: 10.1103/PhysRevB.63.165406 PACS number(s): 68.37.Lp, 61.46.+w, 71.15.Pd

I. INTRODUCTION

In the past years, material research mainly focused on bulk materials and their surfaces in order to understand and to model their behavior under different external conditions. Recently a lot of attention, both from theoretical and from applied point of view, is devoted to clusters deposited on a surface. Deposited clusters are building blocks for nanostructures and nanostructured materials. To obtain insight in the physical properties of such nanosystems, it is necessary to understand the physical and chemical properties of individual clusters.

Various techniques can be applied to study the structural, electronic, and other properties of clusters which can differ strongly from the properties of the corresponding bulk material. The most reliable results are obtained by a combination of experimental and theoretical techniques. In most of these studies the tools needed to model cluster systems at an atomic scale are tested and adapted to predict the properties of bulk materials and, in the best cases, of their surfaces. Therefore the extent to which predictions made by modeling are valid is unclear and a systematic comparison with experiment is necessary.

In a previous investigation,[1] we studied Au clusters deposited by low-energy cluster beam deposition (LECBD) on amorphous carbon and MgO surfaces by high-resolution electron microscopy (HREM) in combination with molecular dynamics (MD). For clusters deposited on MgO, lattice dilations through the different cluster layers were measured. This behavior was modeled with MD and detailed studies showed that the relaxation of the cluster was closely correlated to the cluster morphology and the interaction with the surface on which the cluster was deposited. Other experimental techniques, e.g., low-energy ion scattering (LEIS) (Ref. 2) or x-ray photoemission spectroscopy (XPS),[3] are frequently used in combination with Monte Carlo (MC) simulations to study, e.g., segregation effects and alloying behavior in bimetallic cluster systems.

Many bimetallic systems, interesting for catalysis research, have already been studied: Pd-Pt clusters with different chemical compositions,[2,4,5] clusters of Au-Ni,[3] Pd-Au,[6,7] and Pd-Cu.[8,9] Clusters of the first three materials—which are immiscible in bulk quantities—were produced by laser vaporization and deposited by LECBD. The nonequilibrium conditions which govern the cluster formation in the source allow the synthesis of two immiscible metallic compounds, impossible to obtain by conventional techniques. In all of these cluster materials, segregation takes place. For Pd-Pt clusters the formation of a Pd rich surface is reported, and for Au-Ni and Pd-Au clusters there is a phase separation between the surface and the volume induced by a surface Au segregation.

The crystal structure of PdCu and $PdCu_3$ clusters is dependent on the annealing temperature.[8,9] Annealing between 300 and 400 °C produces PdCu particles with a fcc structure. After annealing at 450 °C, they adopt the ordered $L1_0$ structure. Particles of $PdCu_3$ are reported to have the ordered $L1_2$ phase. The $L1_0$ phase and the $L1_2$ phase are the ordered crystal structures for bulk PdCu and $PdCu_3$, respectively. Comparable results were also obtained for Pd-Cu clusters, synthesized by different methods (see references in Ref. 8).

Another well-studied bimetallic cluster system is AuCu. The alloying behavior and the diffusion of Cu in Au clusters as function of temperature is described in Ref. 10. The role of the cluster size is discussed as well.[11–13] All these studies are carried out by transmission electron microscopy (TEM).

It is found that at room temperature Cu atoms can quickly dissolve into 4-nm-sized Au clusters to form a homogeneously mixed alloy. At reduced temperatures, a two-phase structure is formed in which a pure Au core is surrounded by a solid solution of Au and Cu. Not only temperature but also the size of the clusters has an effect on the alloying behavior. 4-nm-sized Au clusters on which Cu atoms were evaporated at 300 K are forming homogeneously mixed Au-Cu alloy clusters by a rapid dissolution of the Cu atoms. For 10-nm-sized Au clusters, this rapid dissolution only takes place in a shell-shaped region close to the surface of the cluster; the core is still pure Au. For larger clusters (around 30 nm) no dissolution takes place. After annealing, the larger Cu_3Au clusters (20 and 9 nm) adapt the ordered $L1_2$ structure, while the 4-nm clusters still form a homogeneously mixed solid solution. In Ref. 12 this behavior was explained by a lowering of the order-disorder transition temperature (T_c).

Since we found that HREM was successful in characterizing low-energy-deposited pure Au clusters which properties could be simultaneously studied by atomic scale modeling, it is worthwhile to extend this combined investigation to the case of Au-Cu deposited clusters. This paper deals with the crystal structure and chemical composition of different Au-Cu alloy clusters prepared by laser vaporization starting from different Au-Cu alloy targets. The clusters are deposited by LECBD on amorphous carbon and MgO cubes. Not only the matching between experiment and MC modeling is discussed, also the discrepancies between experiment and theory are pointed out and will be discussed.

There are several reasons why the Au-Cu bimetallic system was chosen. One reason is that bulk $Cu_{1-x}Au_x$ alloys are well known. Three stable phases are identified at room temperature. The structure is $L1_2$ for x around 0.25 and x around 0.75; in the vicinity of $x=0.5$ the structure is $L1_0$. The phase at $x = 0.25$ is characterized by a first-order order-disorder transition temperature $T_c=663$ K. Since this temperature can be reached without any experimental difficulty, this phase transition is observed by means of several techniques. It also stimulated the interest of atomic scale modeling and the combination of both the experimental and modeling approach. However, the antisite energy in $L1_2$ $Cu_{1-x}Au_x$ alloys is particularly high and, even at elevated temperatures, site exchanges are unlikely events. Therefore MD sampling is inadequate and the MC atomic scale methods are preferred.

Available cohesion models turned out to be accurate enough to allow reasonable predictions of the order-disorder phase transition temperature of Cu_3Au. The wetting of the ordered phase by a disordered phase at antiphase and twin boundaries was evidenced by TEM at a temperature below T_c.[14] MC simulations successfully reproduced this wetting phenomenon.[15] The relaxation of the atomic positions in the vicinity of a $\Sigma=5$ (210) [100] tilt boundary was evidenced and measured by HREM; it was also studied in detail by MD.[16] Beyond relaxation, the order at the same interface was thoroughly studied by MC sampling as a function of temperature.[17] This modeling study was extended to surfaces and compared to experiment.[18]

Another reason for this investigation is that although Au-Cu alloy clusters have been studied before, the production methods in these cases were very different.[10–13] In our case Au-Cu clusters are produced as a whole in the source, outside thermodynamic equilibrium, and afterwards deposited with low energy on different surfaces—amorphous carbon and crystalline MgO cubes—at the same time.

The paper is structured as follows: Sec. II describes the experimental techniques; in Sec. II A the cluster production and deposition is explained and in Sec. II B the electron microscopy techniques are presented. Section III contains the overview of the techniques to model the Au-Cu system, Sec. IV a discussion of the results, and in Sec. V the conclusions are presented.

II. EXPERIMENTS

A. Production and deposition of clusters

The binary clusters are fabricated in a laser vaporization cluster source. The source and its operation are described in full detail in Ref. 19. Briefly, pulsed laser vaporization is used to create a plume of atoms, dimers, and small clusters, while simultaneously He carrier gas under high pressure is pulsed into the source chamber. The vaporized material then merges with the carrier gas. This mixture stays in the waiting room for a short period after which it expands supersonically through a nozzle into the vacuum. During this process the atoms condense into clusters. The cluster beam production is repeated at a frequency of 10 Hz. Characteristic for laser vaporization cluster sources is that the metal vapor is quenched, producing a cold beam of clusters with a temperature lower than 300 K and a cluster kinetic energy below 1 eV/atom. This makes the clusters suited for LECBD.[20–22] The clusters have not yet reached their equilibrium size and shape. Therefore no magic numbers are observed in the mass spectrum.

Several procedures can be followed for the production of binary metal clusters, e.g., simultaneous vaporization of different metal targets by different laser pulses allows production of clusters with adjustable composition, even for mixtures that are not readily available as bulk metals (see Ref. 19 and references therein). Here we opted for a different approach: bulk alloys were used as target material. Three different compositions of Au and Cu were employed: Cu 25 at. %-Au (Au_3Cu), Cu 50 at. %-Au (CuAu), and Cu 75 at. %-Au (Cu_3Au). The cluster production, i.e., the size distribution, abundances, and yield, crucially depends on various experimental parameters. An ablation laser energy of approximately 25 mJ per laser pulse and a He gas pressure of about 8.5 bars were used. In the experiments presented here the clusters, neutrals as well as ions, were deposited as prepared directly from the frozen metal vapor.

Both the cluster size distribution and the chemical composition of the clusters were analyzed in flight with a reflectron-type time-of-flight mass spectrometer. The cluster size distribution for the present study was very analogous to the one presented in our earlier study on Au clusters,[1] and typically ranged from the monomer up to clusters with several hundreds of atoms. From the mass spectra the chemical purity and information on the relative Au and Cu content in

the clusters was deduced. For all clusters sizes that still could be resolved, chemical contaminations were limited to a single H or O atom.[23] A quantitative characterization of the relative Au and Cu content in individual cluster sizes was, however, only possible for very small clusters, because the mass of a Cu trimer nearly equals the mass of a Au atom. For clusters containing less than ten atoms, however, the bulk target composition was fully reflected in the mass spectra. This, and similar observations for laser vaporization production of other binary clusters from alloy samples,[2–5] made us confident that the alloy composition will to a high degree be reflected in the cluster composition.

For the sample preparation a microscope grid covered with amorphous carbon on which MgO cubes are deposited, is placed on the substrate holder in the cluster source collecting the Au-Cu clusters. Details on the preparation of the MgO cubes on the amorphous carbon are given in Ref. 1. The clusters are deposited on the substrate with low coverage, allowing the individual deposited clusters to be distinguished. After deposition the sample is transferred to the transmission electron microscope. Both the Au-Cu alloy clusters simultaneously deposited on the MgO and the amorphous carbon are studied by electron diffraction (ED) and HREM.

B. Transmission electron microscopy

Diffraction experiments are performed with a Philips CM20 microscope (200 keV). Diffraction patterns are taken from 1-μm^2 areas of clusters on an amorphous carbon support. Because the orientation of the clusters is random, ring patterns result. Rotational averages of the diffraction patterns for the different Au-Cu alloy clusters are calculated. These averages are taken around the central beam. The output is a one-dimensional line scan where the diffraction lines are visible. Also weaker lines induced by an eventual ordering in the Au-Cu alloys would become more apparent.

Diffraction only gives average information about the clusters but local information in real space can only be obtained by HREM of the individual clusters. It is already pointed out in Ref. 1 that the clusters deposited on amorphous carbon or crystalline MgO, do not coagulate and individual clusters are observed. HREM images are obtained with a JEOL 4000 EX microscope with a point resolution of 1.7 Å , and are carried out at low electron beam irradiation density (17 pA/cm^2) to avoid structural changes and reorientations. For HREM orientation of the clusters always has to be along a low index zone axis such as [100] or [011]. If there is a chemical ordering of Au and Cu atoms, this will be visible on the HREM images and also on the fast Fourier transforms (FFT) of these images, where reflections due to the ordering will appear. Prior to the FFT's, a Gaussian mask is put over the HREM images to cover the borders of the cluster. Information about the structure of the cluster will be better visible because information from the borders and the amorphous carbon will be filtered away.

The diffraction signal of the crystalline MgO is much higher than the signal from the deposited clusters and therefore no clear diffraction patterns of clusters deposited on the MgO cubes can be obtained. Information about the ordering of Au-Cu alloy clusters deposited on MgO is exclusively obtained by HREM. Because of the epitaxial relation between the MgO substrate and the Au-Cu alloy clusters, it is easy to orient the MgO cubes along a low index zone axis and to image both at high magnification.

Simulations of HREM images are obtained using the EMS program[24] running on a DEC alpha XP 1000 Workstation. The clusters are placed in a square supercell of 4.5 nm in the x and y directions perpendicular to the zone axis which is taken as the z direction. Care is taken that the supercell is large enough so that no influence of its borders is introduced on the image. The supercell is divided in the z direction in slices of 1.5 Å thickness. First, the electron wave function of the model is calculated with a multislice dynamical calculation. The sampling in the x and y direction is always 512 pixels in each direction, which gives a precision of 8.8 $\times 10^{-2}$ Å between two neighboring pixels. Second, the HREM images are calculated using the electron wave function and the microscope parameters (spherical aberration constant $C_s = 1$ mm, defocal spread $\Delta f = 8.0$ nm, semiconvergence angle $\alpha = 0.55$ mrad) as input.

Diffraction patterns of pure Au clusters and different Au-Cu alloy clusters deposited on amorphous carbon are shown in Fig. 1. As inset in every diffraction pattern, the line plot obtained by rotational averaging is shown. All rings can be indexed on a fcc lattice. A number of clusters, preferably in a $\langle 011 \rangle$ orientation, are imaged and studied. The average size of the clusters ranges from 1.0 to 4.5 nm. Figure 2(a) shows an image of a CuAu cluster deposited on amorphous carbon: it has the morphology of a cubo-octahedron. Figure 2(b) is the corresponding FFT. Also decahedral clusters are frequently observed; along [011] their fivefold symmetry is clearly reflected. Besides clusters with these two morphologies, which are easily recognized, also clusters with no special morphology are observed. Very often they are twinned.

To study the morphology of the clusters deposited on MgO, different projections of the cluster perpendicular to the interface cluster/substrate are presented. Figures 3(a) and (c) show two different cross-section images of Cu_3Au clusters deposited on MgO: Fig. 3(a) is a cluster in a $\langle 011 \rangle$ orientation while the cluster depicted in (c) is oriented along the $\langle 001 \rangle$ zone axis. Figure 3(b) is the FFT of the cluster shown in Fig. 3(a).

III. MONTE CARLO MODELING

A. Method

First we want to predict the properties of free small clusters and second we want to study the effects which an interfacial distortion, resulting from a lattice mismatch, may induce. The experimentally observed clusters are mostly truncated octahedra, for which modeling is straightforward. The composition, however, is not accurately known nor the spatial distribution of Cu and Au.

Ordering and segregation are studied at the atomic scale by Metropolis Monte Carlo (see, e.g., Ref. 25). This method was recently employed to study structural and thermody-

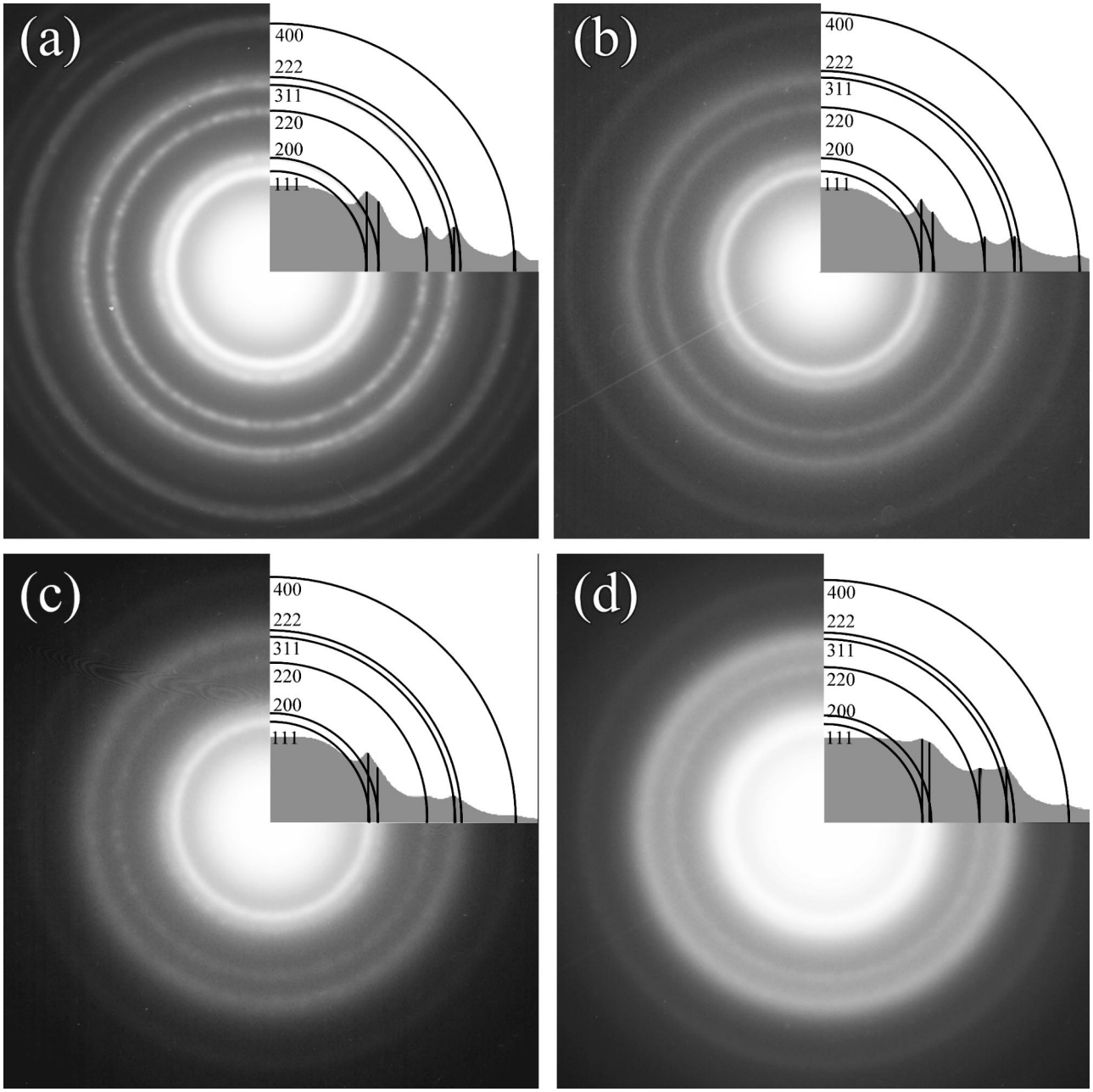

FIG. 1. Diffraction patterns of Au (a), Au_3Cu (b), CuAu (c), and Cu_3Au (d) clusters deposited on amorphous carbon. The rotational averages of each diffraction pattern are shown as an inset.

namic properties of $Ni_{1-x}Al_x$ clusters as function of x.[26] In the presented work a similar scheme will be used.

We employ the MC method in the so-called ''modified grand-canonical ensemble with transmutations'' ($\Delta\mu NPT$).[27] In this approach the total number of the particles ($N=N_{Au}+N_{Cu}$), temperature (T), pressure (P), and chemical potentials difference ($\Delta\mu=\mu_{Au}-\mu_{Cu}$) are fixed. The partial number of each kind of atoms (N_{Au}, N_{Cu}) may be changed. The method includes trials on atomic moves, site exchanges, and chemical nature changes. A trial on structural and volume modifications of the unit cell is also included. The details of the algorithm are given in Ref. 26.

Acceptance is based on estimates of configuration energy differences. The cohesive energy of the systems is estimated on the basis of the second moment tight-binding approximation[28] and is written as

$$E_i=\frac{1}{2}\sum_{i\neq j}\varphi_{\alpha\beta}(r_{ij})-\sqrt{\sum_{i\neq j}\Phi_{\alpha\beta}(r_{ij})}. \qquad (1)$$

In Eq. (1), α and β refer to the chemical nature of the interacting atoms. For the functions $\varphi_{\alpha\beta}$ and $\Phi_{\alpha\beta}$, we adopt the functional dependencies suggested for bulk materials in Ref. 29. These functions are formed by cubic spline segments limited by cutoffs bringing the resulting forces to a range slightly beyond the third neighbor distance. This model was

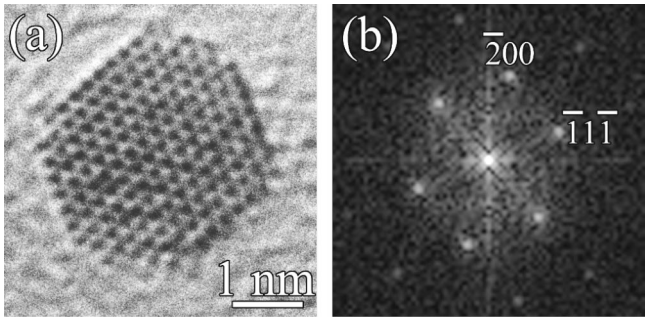

FIG. 2. HREM image of a CuAu cluster in the [011] orientation deposited on amorphous carbon and its corresponding FFT: (a) The cluster has the morphology of a cubo-octahedron; (b) fast Fourier transform from (a).

found to predict a reasonable critical temperature for the first-order order-disorder phase transition in the Cu_3Au bulk phase.[17]

In addition, to model lattice distortions similar to those imposed by the MgO lattice on the clusters, an additional harmonic potential is applied to the interfacial copper and gold atoms. It is given as

$$U_i^H = \frac{1}{2} k (\Delta r_i)^2, \tag{2}$$

where i is the atomic label and Δr_i is the distance between atom i and the closest MgO expitaxial site. Like in Ref. 1 where MD was employed rather than MC, the constant k is tuned to estimate the influence of the magnitude of the cluster distortion on its properties.

B. Free clusters

The equilibrium composition and structure of a binary alloy A_xB_y can be determined at constant N, P, T, and $\Delta\mu$. This was done for bulk $Cu_{1-x}Au_x$ with x around 0.25 by fixing $\Delta\mu$ at several different values[17] and using the MC method to find the corresponding thermodynamic equilibrium state. The same procedure is used here for a truncated octahedral cluster similar to that found experimentally, and a second one, which only differs from the first by an additional atom layer on all sides. The former contains 454 atoms and the latter 786 atoms. A free spherical cluster containing 959 atoms is considered as well.

The Au concentration x is estimated and represented in Fig. 4 at zero pressure and temperature $T=300$ K as a function of $\Delta\mu=\mu_{Au}-\mu_{Cu}$. The results for the 786-atoms cluster are not displayed since they are similar to the others. A distinction is made between the whole cluster, its core, and a mantle, which surrounds the core. Figure 4 provides several pieces of information about the whole clusters and their cores. Considered as a whole, the clusters display no stable phase at $x\sim0.25$ and they look like a solid solution, whatever x. On the other hand, the spatial distribution of Au is not homogeneous. Indeed, when the overall composition corresponds to $x=0.25$, that is, when $\Delta\mu=-0.475$ eV, it is deduced from the data in Fig. 4 that the core is Au deficient, while the mantle is Au rich. In the mantle, x is a monotonous function of $\Delta\mu$, while it displays a plateau value in the core at $x\sim0.23$ for $-0.45\text{ eV}<\Delta\mu<-0.35$ eV. In other words, a stable phase is evidenced in the core, which turns out to have a $L1_2$ structure. The mantle, where the excess Au is located, has a fcc (disordered) structure.

The cubic $L1_2$ structure can be described as a stacking of {100} planes: one formed half by Cu, half by Au and the second formed only by Cu. Hence the concentration of Cu, η_{Cu}, averaged over all second planes can be used as an order parameter. It is represented in Fig. 5 as a function of temperature for the two octahedral clusters considered. The chemical potential difference is fixed at $\Delta\mu=-0.4$ eV, which corresponds to the middle of the plateau in Fig. 4.

In contrast with the first-order phase transition observed in bulk Cu_3Au and predicted with the same potential,[17] order in small clusters is a smoothly decreasing function of temperature, which is the signature of a second-order phase transition. The core is predicted to be fully ordered at 300 K, while full disorder ($\langle\eta_{Cu}\rangle=0.75$) is only reached at a temperature close to 600 K.

In the case of Cu_3Au clusters deposited on amorphous carbon, clusters are found to be disordered, even at low temperature, when their diameter is smaller than 5 nm.[13] The diameter of our model free cluster is significantly smaller than this limit.

C. Strained clusters

One factor which may promote disorder is the interfacial stress and we therefore consider a distortion, as it might occur when the cluster is deposited on a crystalline surface. A lattice mismatch may induce a lattice distortion for accommodation.[1] This mismatch is particularly large at the Cu_3Au (001)/MgO (001) interface (11.7%), and we now explore its consequence on the cluster structure and order.

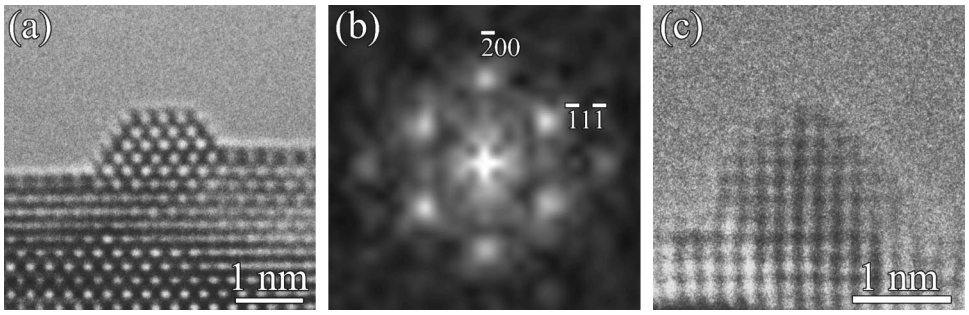

FIG. 3. Cu_3Au clusters deposited on crystalline MgO: (a) A cluster in cross section in the [011] orientation; with the corresponding FFT shown in (b); (c) Image of a cluster with the same morphology as in (a), but now viewed in the [001] orientation.

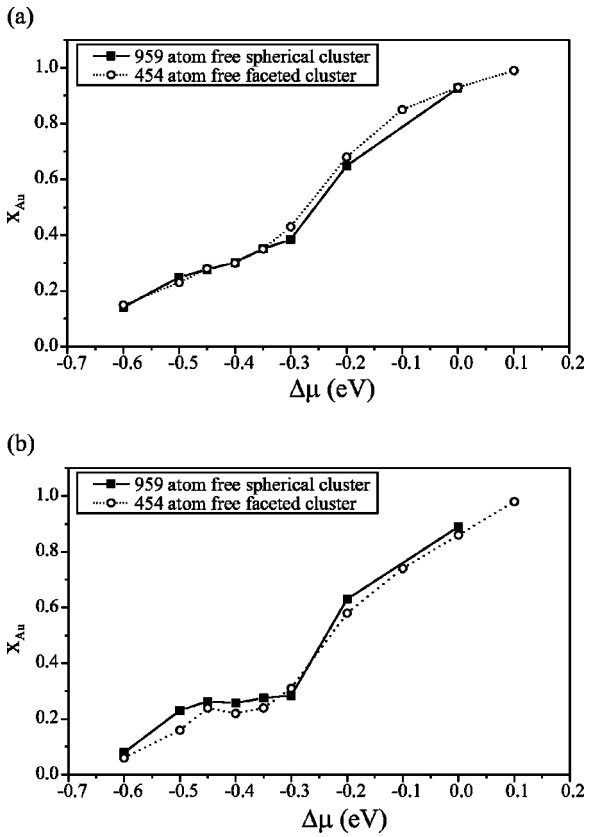

FIG. 4. The concentration of Au in the whole cluster (a) and the core (b) of the cluster vs chemical potential difference ($T=300$ K).

A harmonic potential [Eq. (2)] is added to each atom in the interfacial Cu_3Au plane, and monitored by the force constant k. This way, Cu and Au atoms are constrained toward the MgO expitaxial sites and since the force constant is a parameter, the strength of this constraint can be tuned.

For the largest k value considered ($k=1.0\times10^5$ J/m^2) the first neighbor distance in the interfacial plane of a pure Au cluster will become 2.96 Å, similar to the equilibrium value

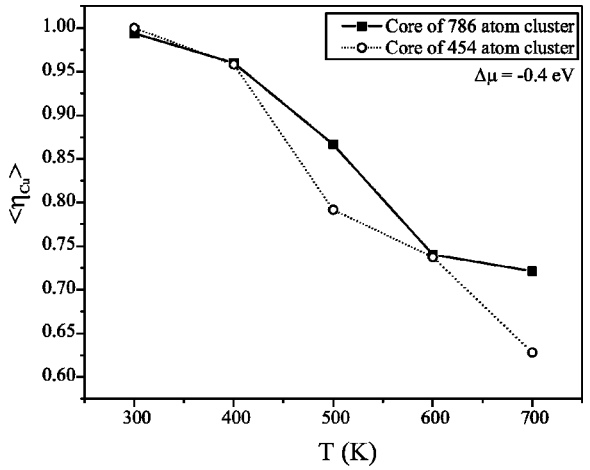

FIG. 5. The average order-disorder parameter (the mean Cu concentration over all second layers) vs the temperature in the core of free clusters of 454 atoms and 786 atoms.

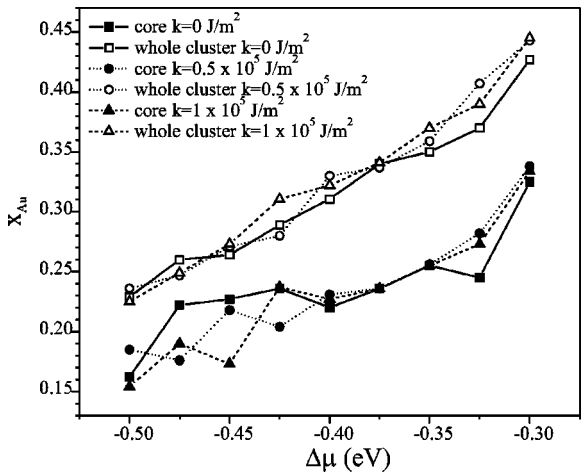

FIG. 6. Au concentration (in the core and in the whole cluster) vs chemical potential difference in the $Cu_{1-x}Au_x$ 454 atoms cluster, that is supported on MgO. The values of the elastic constant of the harmonic potential k are varied from 0 to 1.0×10^5 J/m^2.

in MgO.[1] This distance is only 2.73 Å in the Cu_3Au cluster. When $k=0$ J/m^2 (free cluster), the first neighbor distance in the interfacial plane of the cluster is 2.59 Å while it is 2.64 Å in its core. The interfacial layer expansion is thus quite significant (between 5 and 6%). An expansion results from the harmonic constraint in the whole cluster, which is less than 0.5% in its core. This relaxation is at the limit of the present statistical uncertainties and it is not analyzed in further detail.

To predict the occurrence of an ordered phase, the Au concentration is evaluated as a function of $\Delta\mu$ at 300 K in the same cluster for different values of k. The results are shown for $k=0,0.5\times10^5$ and 1×10^5 J/m^2 and they are displayed for comparison in Fig. 6. The results for the core and the whole cluster are distinct. The effect of the interface distortion is clearly to decrease the stability of the $L1_2$ phase in the core and no phase stability of the Cu_3Au cluster appears when it is epitaxial to the MgO substrate. The segregation state in the mantle is not significantly affected.

The dependence of order on the interface distortion is shown in Fig. 7. The order parameter, averaged over the whole cluster or over the core, is displayed for the 454 atoms supported cluster at room temperature as a function of k. The order parameter measured for the whole cluster is a regularly decreasing function of k. The consequence of Au segregation is that it decreases below its bulk Cu_3Au values ($\langle\eta_{Cu}\rangle=0.75$). The results in Fig. 7(b) show that in the core, order survives limited interfacial deformation. Full disorder in the core is only reached for k values larger than 1.0×10^5 J/m^2, that is, for an interfacial deformation larger than 5%. Hence this MC modeling predicts the tendency for the cluster to fully disorder if accommodating epitaxially to the MgO substrate.

IV. DISCUSSION

A. Morphology

A cluster is a physical system limited in three dimensions, characterized by a given morphology and a large surface to

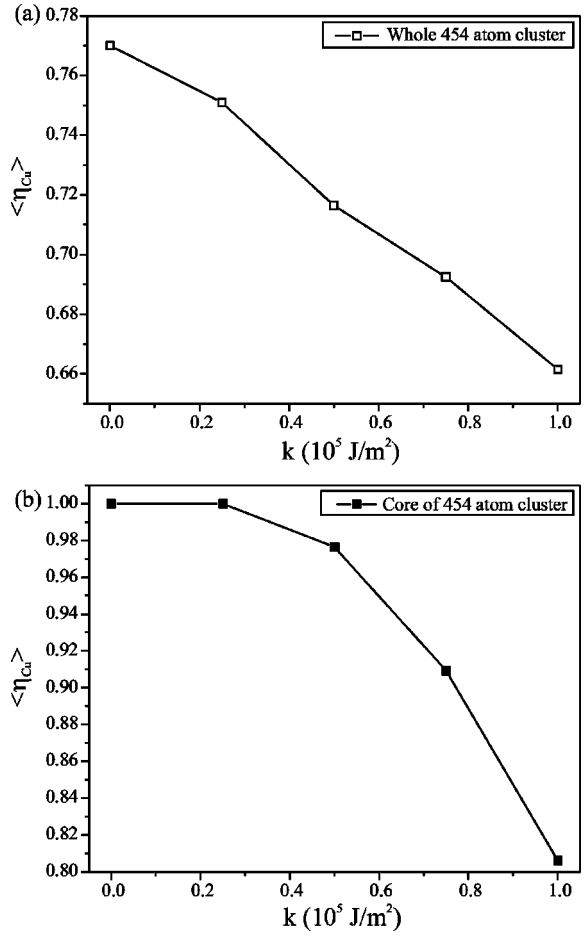

FIG. 7. The average order-disorder parameter (the mean Cu concentration over all second layers) vs the elastic constant k in the cluster taken as a whole (a) and in the core (b) of the 454 atoms supported cluster at room temperature.

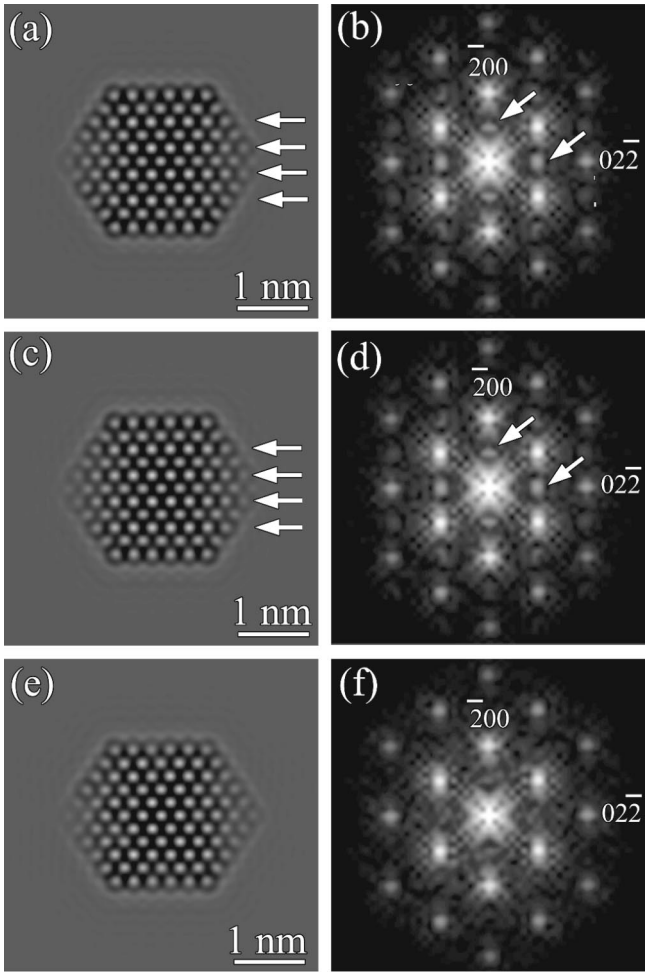

FIG. 8. HREM image simulations of a Cu_3Au cubo-octahedron along the [011] zone axis and the corresponding FFT's: three different models are used: Model I [image (a) and FFT (b)] is the model calculated by MC, model II [image (c) and FFT (d)] is the model where the core and the mantle of the cluster are ordered. Model III [image (e) and FFT (f)] models a cluster, which is chemically disordered in the mantle and the core.

volume ratio. This morphology as well as the surface to volume ratio play an important role in several properties such as, e.g., the kinetics of heterogeneous catalysis. As is pointed out for elemental clusters, this morphology is dependent on the interaction between the cluster and the substrate.[1] Figure 2(a) shows a cubo-octahedral cluster, viewed along the ⟨011⟩ orientation. This morphology is often observed for clusters deposited on amorphous carbon. Also decahedral clusters aligned along the [011] zone axis, are frequently observed. Besides clusters with these two morphologies, which are easily recognized, clusters with no special morphology are also observed. Very often they are twinned.

The morphology of the Au-Cu alloy clusters deposited on MgO cubes is different from those of alloy clusters on amorphous carbon. The profile of Fig. 3(a) is limited by two ⟨112⟩ directions and two ⟨011⟩ directions, while the cluster in a ⟨001⟩ orientation [see Fig. 3(c)] is limited by two ⟨011⟩ directions and four ⟨001⟩ directions: two directions parallel to the interface and two ⟨001⟩ directions perpendicular to the interface. These side truncations of the cluster are only visible when the cluster is aligned along a ⟨001⟩ zone axis orientation. The observed profiles are characteristic for truncated half octahedral clusters. These shapes are confirmed by top view images, that provide projections of the clusters along a ⟨101⟩ or a ⟨110⟩ direction.

The morphologies found for alloy clusters deposited by LECBD on amorphous carbon and MgO, are similar to the elemental ones synthesized by atomic evaporation[30,31] and LECBD.[1] In the case of the Au clusters described in Ref. 1, the largest clusters on MgO have a truncated octahedral morphology. Similarly to small Au clusters (see Fig. 8 in Ref. 1), the Au-Cu alloy clusters are predominantly truncated half octahedra. The morphology of a cubo-octahedron is also observed in Ref. 4 for Pd-Pt clusters deposited on amorphous carbon.

All clusters deposited on MgO show the same epitaxial relation: $(001)_{MgO}//(001)_{Au\text{-}Cu}$ and $[100]_{MgO}//[100]_{Au\text{-}Cu}$. This epitaxial relation was also observed in several other experiments[1,31,32] on Au clusters and is considered as the most stable one. Although the mismatch between the lattice parameters of the different Au-Cu alloy clusters and MgO is much higher than the mismatch between Au and MgO—

11.7% for Cu_3Au, 9.9% for CuAu, and 8.5% for Au_3Cu instead of 2.9% for Au and MgO—the same epitaxial relation is still observed.

B. Ordering

The phase diagram of Au-Cu is well known for bulk materials. Because of the clusters' reduced dimensionality, their phase diagrams, and thus phase stability, may be different.

Figure 1(a) shows the diffraction pattern of an agglomeration of pure Au clusters. This pattern can be indexed as face-centered cubic (fcc) with a lattice parameter of 4.07 Å . This matches perfectly with the bulk structure known for Au.[33] When comparing the diffraction patterns of the different Au-Cu alloys with the diffraction data of Au, it is seen that always the same ring patterns are obtained. Only the lattice parameter differs for all three materials. The Au-Cu clusters all have a face-centered cubic structure with a lattice parameter of 3.87 Å (Au_3Cu), 3.82 Å (CuAu), and 3.76 Å (Cu_3Au). For these three materials, no evidence for a chemical ordering of Au and Cu atoms is found in the diffraction data.

Comparing the diffraction data of the Au-Cu alloy clusters with their corresponding bulk material, it is seen that their lattice parameters match. The crystal data of the solid solution Au-Cu bulk material matches well the results found for the Au-Cu alloy clusters: e.g., the bulk solid solution of AuCu has a lattice parameter of 3.872 Å while the lattice parameter of AuCu clusters is found to be 3.82 Å.

The lattice parameter of Au-Cu alloy clusters apparently diminishes with increasing Cu content in the same way as the bulk material does. Since also the magnitude of the lattice parameters fits, it is therefore assumed that the chemical composition of the clusters corresponds to the chemical composition of the target material in the source. We can thus state that with laser vaporization of an alloy target material, clusters of the same overall chemical composition are formed. The fact that the overall concentration of both elements in the clusters, deposited by LECBD, corresponds to the concentration of the elements of the target material was already observed in Refs. 2, 4, and 5 for Pd-Pt and in Ref. 3 for Au-Ni by means of EDX.

The cluster composition being known, we now address the question of order. Neither by HREM nor in the corresponding FFT's is any evidence found for a chemical ordering between Au and Cu. None of the HREM images taken from clusters—deposited on amorphous carbon or on MgO—of Au_3Cu, CuAu, or Cu_3Au [see Figs. 2(a) and 3(a)] show any superstructure in the $\langle 200 \rangle$ or $\langle 022 \rangle$ directions, which should occur in case of chemical ordering.[34] In the FFT's, the chemical ordering would give rise to extra reflections as, e.g., 100 and $01\bar{1}$; which are extinct in a fcc diffraction pattern. These extra reflections are not observed in any of the FFT patterns [see, e.g., Fig. 2(b) for a CuAu cluster deposited on amorphous carbon, or in Fig. 3(b) for a Cu_3Au cluster deposited on MgO]. All the FFT's give evidence of a regular $\langle 011 \rangle$ face-centered-cubic crystal.

It can be concluded, both from diffraction data as well as from HREM images and their corresponding FFT's, that for Au-Cu clusters deposited on amorphous carbon as well as on crystalline MgO, the crystal structure is fcc. This contrasts with phase diagram predictions for the corresponding bulk material. The same disorder in Cu_3Au clusters deposited on amorphous carbon is found even at low temperature, when their diameter is smaller than 5 nm.[13] The presently identified Au_3Cu crystal structure is also observed in Ref. 35. Also Pd-Cu clusters, deposited on MgO, and annealed at temperatures between 300 and 400 °C are found to be fcc.[8,9]

MC predicts for free Cu_3Au clusters that, seen as a whole, the cluster can be considered as disordered ($\langle \eta_{Cu} \rangle = 0.75$) but in the core the cluster is fully ordered (see Fig. 7 for $k = 0$ J/m^2). Hence the question: What does the HREM image reflect, an overall cluster information which, according to Fig. 7(a) is similar to disorder or information of the core which is predicted by MC as ordered? Maybe the chemically ordered part is too small to contribute substantially to the image and the most important contribution to the image comes from the chemically disordered mantle of the cluster. Another possible reason why the ordering is not seen in the HREM images could be that the cluster itself is too thin to induce the superstructure contrast. To investigate these possibilities image simulations of the cluster calculated by MC (cluster model I) are made. Also two other models are built: cluster model II was chemically ordered in the core and the mantle and cluster model III was completely chemically disordered. For these two cluster models, the same atom positions as for the cluster calculated by MC were used.

The resulting images, calculated at a focus of -65 nm (Scherzer focus at -49 nm), are presented in Fig. 8. Figure 8(a) is the simulated image of the cubo-octahedron as calculated by MC, Fig. 8(c) is the simulated image of cluster model II, and Fig. 8(e) is the simulated image of cluster model III. The corresponding FFT's are given in Figs. 8(b), (d), and (f), respectively. The difference in image between the chemically ordered and chemically disordered cluster [Figs. 8(c) and 8(e)] is clearly seen along the indicated arrows. In the $\langle 200 \rangle$ and the $\langle 022 \rangle$ directions, the ordered cluster gives an image contrast of alternating bright and dark lines. The bright lines in the $\langle 200 \rangle$ direction are marked by arrows in Figs. 8(a) and 8(c). This alternating bright-dark contrast is not seen in the image of the chemically disordered cubo-octahedron. In Fourier space, this extra contrast gives rise to the appearance of the reflections 100 and $01\bar{1}$ (arrowed), which are not present in the Fourier space of the chemically disordered cluster, which shows an fcc $\langle 011 \rangle$ pattern.

Comparing the simulated image of cluster model I [Fig. 8(a)] with the other two images, it is clear that the image of the modeled Cu_3Au cubo-octahedron resembles very well the image of the chemically ordered cubo-octahedron shown in Fig. 8(c). Also here the alternating bright-dark contrast in the two perpendicular directions $\langle 200 \rangle$ and $\langle 022 \rangle$ is visible. Also the Fourier patterns shown in Figs. 8(b) and 8(d) are very alike: both display reflections at the positions 100 and $01\bar{1}$. Image simulations at other defocus values (focus range from -40 to -75 nm with steps of -5 nm) are performed and comparable results are obtained.

All these image simulations indicate that the ordering of the Au and Cu atoms in the core of the cluster should be visible in HREM images and their FFT's. The predicted segregation of excess Au to the mantle of the cluster cannot be resolved in HREM images. These results show that there is still a fair difference between the experimental results and the predictions obtained by MC.

The differences found between the experiments and the MC simulations can have several reasons. First of all the production and deposition processes are not taken into account in the MC modeling. The fact that the clusters are produced out of thermodynamic equilibrium may influence the crystal structure. The size and the temperature of the clusters are also important parameters. Details of the interfacial interaction are also not known. Finally, the cohesion model, designed for bulk systems may not be suited for systems as small as clusters.

We now discuss these possible reasons of divergence. When clusters are produced in the cluster source, the plasma formed by the laser vaporization of the target material, is rapidly cooled by the He gas pulse in the chamber. Further cooling is achieved through a supersonic expansion into vacuum. This quenching can cause solid solution clusters to be formed. The same behavior is found in bulk materials which are heated and then quenched within a short time as compared to the evolution time to equilibrium. The mass spectra do not exhibit magic numbers, which indicates that the clusters are indeed formed out of equilibrium. It may be noticed, however, that, despite of the deviation from equilibrium, bimetallic clusters formed by elements which are not miscible at a macroscopic scale, e.g., Au-Ni, Pd-Pt, or Pd-Au, do not mix in the corresponding clusters.[2–7]

Another important step in the cluster production process, which is also not accounted for in the MC modeling, is the deposition on amorphous carbon or on crystalline MgO. Within the first few picoseconds of the impact, the clusters are heavily destroyed.[36,37] The substrate structure and the electron-phonon coupling govern the later evolution of the cluster. This heavy perturbation may induce atomic rearrangements, and thus enhance the separation between nonmiscible species as well as the mixing of miscible elements. Besides these thermodynamic aspects, chemical interactions need to be considered. When the clusters are deposited on a MgO surface, there is the possibility that some Cu atoms will form bonds with O atoms of the surface, which may influence the crystal structure of the cluster. Similarly, when the clusters land on the amorphous carbon substrate, bondings between Cu and C atoms can form. The relation between such bond forming with strain and segregation is not known.

Size effects are considered in Ref. 12. Cu_3Au clusters of different sizes are heated to 573 K and then slowly cooled down to room temperature. Afterwards, the crystal structure and the chemical ordering of clusters with sizes of 4, 9, and 20 nm are studied. It is found that the 4-nm-sized clusters are fcc; no chemical ordering takes place during annealing. For the larger clusters, the ordered $L1_2$ phase is observed. This means that the size of the cluster influences the crystal structure. In Ref. 12, this behavior was explained by a lowering of the order-disorder critical transition temperature because of a decreasing Debye temperature for small systems. For clusters of 4 nm, this transition temperature is suggested to become so low that the crystal structure becomes fcc instead of $L1_2$. With the present MC model, a first-order phase transition is indeed predicted for bulk materials.[17] It is predicted here to become a second-order transition for small systems (see Fig. 5).

We now address the problems of the cohesion model. The atomic scale cohesion model is based on Eq. (1), initially established for bulk transition metals within the second moment tight-binding approximation.[28] This approximation is consistent with the Friedel theory for transition metals in which the cohesion energy scales with the filling of the *d* band. In many circumstances, however, the functional dependence in Eq. (1) is found to work well for other metals provided a suitable parametrization is found. This is the case of the Cu_3Au bulk alloy for which macroscopic mechanical and thermodynamic properties are well predicted. There still remains an open question, however: whether to which extent a parametrization based on macroscopic properties is valid at a nanoscale. As discussed in Ref. 26 and references therein, quantum effects are not expected to be significant for systems of the size considered in this work. However, surfaces, arrays and vortices induce a strong local decrease of coordinance and subsequent electronic reconfiguration. When the surface to volume ratio is large, as is the case for clusters, this reconfiguration may induce a change in electron hopping integrals that contributes to the cohesion. This effect was already suggested to enhance segregation in Pd bimetallic cluster systems.[4,38] The present difference between observation and MC predictions with Eq. (1) parametrized for bulk Cu_3Au suggests that the decrease of coordinance at the cluster surface may also influence the ordering properties in its core.

V. CONCLUSIONS

Au-Cu alloy clusters were produced by a laser vaporization source with different compositions (Au_3Cu, CuAu, and Cu_3Au) as target material. Afterwards, the clusters were deposited with low energy on amorphous carbon and crystalline MgO cubes. The deposited clusters were examined by electron diffraction and high-resolution electron microscopy. It is found that the chemical composition of the clusters corresponds to the chemical composition of the target material. Laser vaporization can therefore be considered as a reliable way to produce bimetallic clusters with a uniform composition. Different cluster morphologies are found for different surfaces. On amorphous carbon, cubo-octahedra and decahedral clusters are often observed, also spherical clusters, often twinned, are present. For the clusters deposited on MgO, only truncated half octahedral shapes are found.

From the electron-diffraction patterns as well as from the HREM images, it can be concluded that clusters of Au_3Cu, CuAu, and Cu_3Au all have a face-centered-cubic structure. This points to a chemical disorder between Cu and Au atoms in the bimetallic cluster; a solid solution is formed. The crystal structures for the Au-Cu alloy clusters are thus very dif-

ferent from the crystal structures of the corresponding bulk materials.

Monte Carlo simulations, using the second moment tight-binding approximation, are used to model ordering and segregation in a Cu_3Au cluster. It is found that the cluster contains an ordered core and that the excess Au atoms segregate to the mantle, which is found to be disordered. It is also pointed out that a lattice distortion, e.g., due to a lattice mismatch between cluster and substrate, can destroy the ordering in the core.

Several possible reasons for the differences between the experimental observations and the simulation results were discussed. To get more insight in the bimetallic cluster system and to find the reason for disorder in the clusters, it is necessary to study different nanoalloys, produced in different ways and deposited on different substrates.

ACKNOWLEDGMENTS

B.P. and P.L. are grateful to the Fund for Scientific Research-Flanders (Belgium) for financial support. L.T.K. is grateful for grants from the Danish Research Council (SNF and STVF). This research is part of the Interuniversity Poles of Attraction Program—Belgian State, Prime Minister's Office—Federal Office for Scientific, Technical and Cultural Affairs (IUAP 4/10).

*Corresponding author. Email address: bapauw@ruca.ua.ac.be

†Present address: Department of Experimental Nuclear Physics, St. Petersburg State Technical University, Polyteknicheskaya Street 29, 195251, St. Petersburg, Russia.

‡Present Address: Ørsted Laboratoriet, Niels Bohr Institutet for Astronomi, Fysik og Geofysik, Universitetsparken 5, DK-2100 Køben-havn Ø, Denmark.

§Present Address: Atlas Copco Airpower, Boomsesteenweg 957, B-2610 Wilrijk, Belgium.

[1] B. Pauwels, G. Van Tendeloo, W. Bouwen, L. Theil Kuhn, P. Lievens, H. Lei, and M. Hou, Phys. Rev. B **62**, 10 383 (2000).

[2] J. L. Rousset, A. J. Renouprez, and A. M. Cadrot, Phys. Rev. B **58**, 2150 (1998).

[3] J. L. Rousset, F. J. Cadete Santos Aires, B. R. Sekhar, P. Mélinon, B. Prével, and M. Pellarin, J. Phys. Chem. B **104**, 5430 (2000).

[4] J. L. Rousset, A. M. Cadrot, F. J. Cadete Santos Aires, A. Renouprez, P. Mélinon, A. Perez, M. Pellarin, J. L. Vialle, and M. Broyer, J. Chem. Phys. **102**, 8574 (1995).

[5] J. L. Rousset, B. C. Khanra, A. M. Cadrot, F. J. Cadete Santos Aires, A. J. Renouprez, and M. Pellarin, Surf. Sci. **352-354**, 583 (1996).

[6] R. J. Davis and M. Boudart, J. Phys. Chem. **98**, 5471 (1994).

[7] F. J. Cadete Santos Aires, J. L. Rousset, P. D. Szkutnik, G. Bergeret, and A. Renouprez (unpublished).

[8] S. Giorgio and C. Henry, Microsc. Microanal. Microstruct. **8**, 379 (1997).

[9] S. Giorgio, H. Graoui, C. Chapon, and C. R. Henry, Cryst. Res. Technol. **33**, 1061 (1998).

[10] H. Yasuda, H. Mori, M. Komatsu, and K. Takeda, J. Appl. Phys. **73**, 1100 (1993).

[11] H. Yasuda and H. Mori, Z. Phys. D: At., Mol. Clusters **31**, 131 (1994).

[12] H. Yasuda and H. Mori, Z. Phys. D: At., Mol. Clusters **37**, 181 (1996).

[13] H. Yasuda and H. Mori, Ann. Phys. (Paris) **22**, C2-127 (1997).

[14] F. D. Tichelaar, F. W. Schaping, and X-F. Li, Philos. Mag. A **65**, 913 (1992).

[15] M. El Azzaoui, Ph.D. thesis, ULB Brussels, 1996.

[16] M. El Azzaoui, J-M. Pénisson, and V. Pontokis, Interface Sci. **2**, 79 (1994).

[17] M. El Azzaoui and M. Hou, J. Phys. C **8**, 6833 (1996).

[18] M. Hou and M. El Azzaoui, Surf. Sci. **380**, 210 (1997).

[19] W. Bouwen, P. Thoen, F. Vanhoutte, S. Bouckaert, F. Despa, H. Weidele, R. E. Silverans, and P. Lievens, Rev. Sci. Instrum. **71**, 54 (2000).

[20] P. Jensen, Rev. Mod. Phys. **71**, 1695 (1999).

[21] H. Haberland, Z. Insepov, and M. Moseler, Phys. Rev. B **51**, 11 061 (1995).

[22] W. Bouwen, E. Kunnen, K. Temst, M. J. Van Bael, F. Vanhoutte, H. Weidele, P. Lievens, and R. E. Silverans, Thin Solid Films **354**, 87 (1999).

[23] W. Bouwen, F. Vanhoutte, F. Despa, S. Bouckaert, S. Neukermans, L. Theil Kuhn, H. Weidele, P. Lievens, and R. E. Silverans, Chem. Phys. Lett. **314**, 227 (1999).

[24] P. A. Stadelmann, Ultramicroscopy **21**, 131 (1987).

[25] M. P. Allen and D. J. Tildesley, *Computer Simulation of Liquids* (Clarendon Press, Oxford, 1987).

[26] E. E. Zhurkin and M. Hou, J. Phys. C **12**, 6735 (2000).

[27] S. M. Foiles and M. S. Daw, J. Mater. Res. **2**, 5 (1987).

[28] F. Ducastelle, J. Phys. (Paris) **31**, 1055 (1970).

[29] G. J. Ackland and V. Vitek, Phys. Rev. B **41**, 10 324 (1990).

[30] S. Giorgio, C. R. Henry, C. Chapon, and J.-M. Penisson, J. Cryst. Growth **100**, 254 (1990).

[31] T. Kizuka and N. Tanaka, Phys. Rev. B **56**, R10 079 (1997).

[32] T. Kizuka, T. Kachi, and N. Tanaka, Z. Phys. D: At., Mol. Clusters **26**, S58 (1993).

[33] X-ray Powder Data Files, Sets 1–5, ASTM, p. 571, No. 4-0784.

[34] P. Villars and L. D. Calvert, *Pearson's Handbook of Crystallographic Data for Intermetallic Phases (Second Edition)* (ASM International, Metals Park, OH, 1991), Vol. 1, pp. 1273-1274.

[35] D. K. Saha, K. Koga, and H. Takeo, Nanostruct. Mater. **8**, 1139 (1997).

[36] M. Hou, Nucl. Instrum. Methods Phys. Res. B **135**, 501 (1998); H. Lei, Q. Hou, and M. Hou, *ibid.* **164-165**, 537 (2000).

[37] Q. Hou, M. Hou, L. Bardotti, B. Prével, P. Mélinon, and A. Perez, Phys. Rev. B **62**, 2825 (2000); L. Bardotti, B. Prével, P. Mélinon, A. Perez, Q. Hou, and M. Hou, *ibid.* **62**, 2835 (2000).

[38] J. L. Rousset, J. C. Bertolini, and P. Miegge, Phys. Rev. B **53**, 4947 (1996).